

This is the author's peer reviewed, accepted manuscript. However, the online version of record will be different from this version once it has been copyedited and typeset.

PLEASE CITE THIS ARTICLE AS DOI: 10.1063/1.50198106

1 **Wave interaction with multiple adjacent floating solar panels with arbitrary constraints**

2

3 Yifeng Yang (杨毅锋)^{1,3}, Kang Ren (任康)¹, Binzhen Zhou (周斌珍)⁴, Shi Yan Sun (孙士艳)^{2,a)},

4

Luofeng Huang (黄洛枫)³

5

6 ¹ *Department of Mechanical Engineering, University College London, Torrington Place, London*

7 *WC1E 7JE, UK*

8 ² *School of Naval Architecture & Ocean Engineering, Jiangsu University of Science and*

9 *Technology, Zhenjiang 212003, China*

10 ³ *School of Water, Energy and Environment, Cranfield University, Cranfield, MK43 0AL, UK*

11 ⁴ *School of Civil Engineering and Transportation, South China University of Technology,*

12 *Guangzhou, 510641 China*

13

14 **ABSTRACT**

15 The problem of wave interaction with multiple adjacent floating solar panels with arbitrary types
 16 and numbers of constraints is considered. All the solar panels are assumed to be homogeneous, with
 17 the same physical properties, as well as modelled by using the Kirchhoff-Love plate theory. The
 18 motion of the fluid is described by the linear velocity potential theory. The domain decomposition
 19 method is employed to obtain the solutions. In particular, the entire fluid domain is divided into two
 20 types, the one below the free surface, and the other below elastic plates. The velocity potential in
 21 the free surface domain is expressed into a series of eigenfunctions. By contrast, the boundary
 22 integral equation and Green function are employed to construct the velocity potential of fluid
 23 beneath the entire elastic cover, with unknowns distributed along two interfaces and jumps of
 24 physical parameters of the plates. All these unknowns are solved from the system of linear equations,
 25 which is established from the matching conditions of velocity potentials and edge conditions. This
 26 approach is confirmed with much higher computational efficiency compared with the one only
 27 involving eigenfunction expansion for the fluid beneath each plate. Extensive results and
 28 discussions are provided for the reflection and transmission coefficients of water waves, maximum

^{a)} Corresponding author, E-mail: shiyun_sun@126.com (Shiyan Sun)

This is the author's peer reviewed, accepted manuscript. However, the online version of record will be different from this version once it has been copyedited and typeset.

PLEASE CITE THIS ARTICLE AS DOI: 10.1063/5.0198106

29 deflection and principal strain of the elastic plates, especially, the influence of different types and
30 numbers of edge constraints are investigated in detail.

31

32 I. INTRODUCTION

33 In recent years, photovoltaic (PV), commonly referred to as the solar panel, has emerged as one of
34 the most economically viable renewable energy technologies in history¹. Typically, the deployment
35 of solar panels necessitates vast expanses of land to generate a substantial amount of electricity.
36 However, this can pose challenges in regions where land resources are limited. Furthermore, there
37 is also significant competition for land that serves multiple purposes, including agriculture for food
38 production and conservation efforts to protect biodiversity. Consequently, a pivotal consideration
39 arises regarding the optimal placement of these solar panels². One of the solutions is to deploy
40 floating solar panels at seas³. However, ocean waves may pose a substantial challenge to the
41 effective operation of solar panels. On the one hand, the wave-induced motions of floating solar
42 panels may adversely impact their energy efficiency. On the other hand, large movements or
43 deformation caused by waves may carry the risk of structural damage, resulting in significant
44 economic losses. Therefore, it is necessary to investigate the hydrodynamic properties of floating
45 solar panels in ocean waves.

46

47 Research based on linear theories has been well applied to hydroelasticity, such as sea-ice dynamics
48 and wave-ice-structure interactions, where the linearized velocity potential theory is employed to
49 describe the motion of fluid, and the ice sheet is modelled as a thin elastic plate. In particular, [Fox](#)
50 [and Squire](#)⁴ studied wave transmission and reflection by a semi-infinite floating ice sheet through
51 the method of matched eigenfunction expansions (MEE), where the edge of the sheet was assumed
52 to be free to move. Later, a similar problem was considered by [Balmforth and Craster](#)⁵, where the
53 Timoshenko-Mindlin equation was adopted to describe the ice sheet, and the Wiener-Hopf technique
54 was used to derive the solution. [Meylan and Squire](#)⁶ proposed an approximated solution based on
55 an analytical solution of a semi-infinite ice sheet⁴. [Wu, et al.](#)⁷ studied the same problem and solved
56 it exactly through MEE.

57

58 For multiple floating ice plates, [Sturova](#)⁸ studied the water wave diffraction by a semi-infinite

This is the author's peer reviewed, accepted manuscript. However, the online version of record will be different from this version once it has been copyedited and typeset.

PLEASE CITE THIS ARTICLE AS DOI: 10.1063/5.0198106

59 composite elastic plate, which was modelled as a combination of two ice sheets of different
 60 properties, where one is of finite size and the other is semi-infinite. [Evans and Porter⁹](#) considered
 61 the problem of wave diffraction by an ice sheet fully covering the water surface with a narrow crack
 62 of infinite extent, where the free edge conditions were imposed at the crack. In their work, MEE
 63 and Green function methods were both employed to derive the solution. [Williams and Squire¹⁰](#)
 64 investigated the wave scattering by three floating ice sheets of different properties based on the
 65 method of Wiener-Hopf technique and residue calculus. The works mentioned above pertain to
 66 plates that are either interconnected or separated by minimal gaps. However, there are instances
 67 where the spacing between two plates may be obvious. For example, [Chung and Fox¹¹](#) studied the
 68 reflection and transmission of waves across a gap between two semi-infinite ice sheets. [Shi, et al.¹²](#)
 69 studied the problem of wave diffraction by multiple wide-space ice sheets approximately.
 70 Furthermore, if offshore structures such as ships working in polar regions, the effects of structures
 71 should be further considered. Typically, [Ren, et al.¹³](#) considered the wave-excited motions of a body
 72 floating on water confined between two semi-infinite ice sheets, where the fluid domain was divided
 73 into several sub-regions, and the MEE was applied to match the solution at each interface.

74
 75 The thin elastic plate model and linearized velocity potential theory were also used to study the
 76 interaction between water waves and floating offshore structures. For example, [Karmakar and
 77 Soares¹⁴](#) derived an analytical solution for a floating elastic plate with two edges moored to the
 78 seabed based on MEE, where the mooring lines were modelled as springs to provide extra vertical
 79 reaction. [Mohapatra, et al.¹⁵](#) considered the problem of wave diffraction by a finite floating elastic
 80 plate with an inner compressible force. [Karmakar, et al.¹⁶](#) solved the problem of wave interaction
 81 with multiple articulated floating elastic plates fully covering the entire free surface by using MEE.
 82 Later, [Praveen, et al.¹⁷](#) further extended it to plates of finite size. A more recent work by [Zhang, et
 83 al.¹⁸](#) studied the hydroelastic response of two floating photovoltaic structures over stepped seabed
 84 condition.

85
 86 As discussed above, a considerable volume of studies have been conducted to investigate the
 87 hydrodynamic properties of floating elastic structures. In the context of floating solar panels at sea,
 88 it is observed that their hydrodynamic performance do exhibit certain similarities with ice sheets.

This is the author's peer reviewed, accepted manuscript. However, the online version of record will be different from this version once it has been copyedited and typeset.

PLEASE CITE THIS ARTICLE AS DOI: 10.1063/1.50198106

89 For instance, when an ice sheet or a group of floating solar panels covers a large amount of free
 90 surface region, the structural elasticity in both cases is quite important. Nonetheless, the
 91 hydrodynamic problems for ice sheets and floating solar panels also show discernible differences.
 92 For example, ice sheets inherently exist in nature, and it is common to assume that the edge of sea
 93 ice is free to move¹⁹. By contrast, solar panels are human-made, and their edge conditions are much
 94 more complicated, which should be determined based on the connections between each two adjacent
 95 panels, as well as the mooring lines used in the structure. Besides, ice sheets are normally shown in
 96 nature with diverse physical properties²⁰ (e.g., thickness). By contrast, one floating solar farm
 97 usually consists of solar panels with identical properties. These distinct differences suggest that the
 98 solution procedure developed for issues involving ice sheets may not be entirely suitable and
 99 efficient to solve problems of floating solar panels. In particular, when addressing problems
 100 involving ice sheets of different properties, a conventional approach is to treat the fluid beneath each
 101 ice sheet as a subdomain, and the velocity potential in each subdomain is written into a series of
 102 eigenfunctions with unknown coefficients. Subsequently, the velocity potential can be matched at
 103 each interface by using MEE to solve these unknowns, a typical example is given by *Ren, et al.*¹³.
 104 Although this approach has demonstrated considerable efficacy in numerous applications, it may
 105 not be so numerically efficient for the current floating panels problem we considered in this work.
 106 In the case of the floating solar panels, the problem will be highly computationally demanding if we
 107 choose to follow the regular procedure above to expand the velocity potential into a series of
 108 eigenfunctions in each subdomain, especially when the numbers of panels and constraints are large
 109 or even huge. Therefore, we develop an alternative and more efficient scheme for floating solar
 110 panels, featured by the combination of Green function technique and MEE. In this scheme, by
 111 modelling each floating solar panel as a thin elastic plate with identical and homogeneous properties,
 112 the velocity potential beneath the entire floating solar panels can be constructed from the boundary
 113 integral equation. Through using the Green function corresponding to fluid fully covered by a
 114 homogeneous elastic plate, only line integrals along two interfaces of the free surface and elastic
 115 covers, as well as the jumps at the edges of the plates need to be remained in the boundary integration
 116 equation. In such a case, unknowns only need to be distributed on the velocity potential on two
 117 interfaces and jumps at the edges of elastic plates. Compared with the conventional MEE
 118 procedure¹³, the total number of unknowns is significantly reduced. Moreover, the addition of one

This is the author's peer reviewed, accepted manuscript. However, the online version of record will be different from this version once it has been copyedited and typeset.

PLEASE CITE THIS ARTICLE AS DOI: 10.1063/1.50198106

119 more plate to the system only leads to an increment in unknowns at the newly introduced edge,
 120 which significantly improves the computational efficiency, especially for a floating solar farm with
 121 a significant number of panels. Based on the present procedure, case studies are conducted for three
 122 typical edge conditions, namely, pinned, hinged and free. The effects of edge conditions on the
 123 reflected and transmitted waves, as well as the hydroelastic response of the floating solar panels are
 124 investigated in detail.

125
 126 The work is organized as below. The mathematical model or governing equation and boundary
 127 conditions of the problem are formulated in Sec. II. In Sec. III, the solution procedure is presented.
 128 Then the results and discussions are made in Sec. IV. Finally, conclusions are drawn in Sec. V.

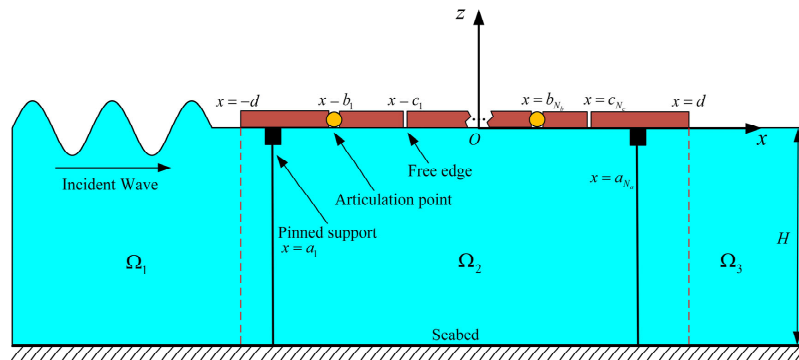


Fig. 1. The sketch of an incident wave interaction with a floating elastic plate.

129

130

131

132 **II. MATHEMATICAL MODEL**

133 In this study, we examine a floating solar farm covering a large horizontal area of open water. Like
 134 many water wave-related problems, we simplify the analysis by considering a two-dimensional
 135 scenario, as illustrated in Fig. 1. In contrast, when the transverse dimension of the structure or fluid
 136 environment is significant to the problem, the three-dimensional effect is important to be considered
 137 (see Yang, et al.²¹, Ren, et al.²²). A Cartesian coordinate system $O-xz$ is introduced, with the x -axis
 138 along the clam water surface and the z -axis pointing upwards. The seabed is located horizontally
 139 along $z = -H$. The water surface region $-d \leq x \leq d$ is covered by multiple floating elastic plates
 140 with homogeneous properties. The density and thickness of the plate are ρ_e and h_e , respectively. In
 141 addition to two side edges at $x = \pm d$, there are also internal constraints between each two adjacent

This is the author's peer reviewed, accepted manuscript. However, the online version of record will be different from this version once it has been copyedited and typeset.

PLEASE CITE THIS ARTICLE AS DOI: 10.1063/1.50198106

142 elastic panels. In particular, the internal pins are applied at $x = a_i$ ($i = 1 \sim N_a$) with $a_i < a_{i+1}$, two
 143 sides of the plate are hinged to each other at $x = b_i$ ($i = 1 \sim N_b$) with $b_i < b_{i+1}$, as well as two sides
 144 of the plate are free to each other at $x = c_i$ ($i = 1 \sim N_c$) with $c_i < c_{i+1}$, as given in Table. 1. An
 145 incoming wave comes from $x = -\infty$ to $x = +\infty$ and will interact with the entire floating solar
 146 panels.

147 Table. 1. Positions of different types of internal constraints of the floating solar panels.

Edge type	Position
Pinned	$x = a_1, a_2, \dots, a_{N_a}$
Hinged	$x = b_1, b_2, \dots, b_{N_b}$
Free	$x = c_1, c_2, \dots, c_{N_c}$

148

149 The fluid with density ρ is assumed to be homogeneous, inviscid, incompressible, and its motion is
 150 irrotational. Under the further assumption made on the small-amplitude motion of the wave, the
 151 linearized velocity potential theory is used to describe the flow. Once the motion is sinusoidal in
 152 time t with radian frequency ω , the total velocity potential can be written as

$$153 \quad \Phi(x, z, t) = \text{Re}\{\phi(x, z)e^{i\omega t}\}, \quad (1)$$

154 where the spatial velocity potential $\phi(x, z)$ contains the incident component $\phi_I(x, z)$ and the
 155 diffracted component $\phi_D(x, z)$. $\phi(x, z)$ is governed by the Laplace equation in the fluid domain,
 156 which can be written as

$$157 \quad \frac{\partial^2 \phi}{\partial x^2} + \frac{\partial^2 \phi}{\partial z^2} = 0. \quad (2)$$

158 The linearized boundary condition on the free surface region can be expressed as

$$159 \quad \frac{\partial \phi}{\partial z} - \frac{\omega^2}{g} \phi = 0, \quad |x| > d, \quad z = 0, \quad (3)$$

160 where g denotes the acceleration due to gravity. The boundary condition on the floating elastic plate
 161 gives

$$162 \quad \left(L \frac{\partial^4}{\partial x^4} - m_e \omega^2 + \rho g \right) \frac{\partial \phi}{\partial z} - \rho \omega^2 \phi = 0, \quad |x| < d, \quad z = 0, \quad (4)$$

163 where $L = \frac{Eh_e^3}{12(1-\nu^2)}$ represents the effective flexural rigidity of the elastic plate, E and ν denote
 164 Young's modulus and Poisson's ratio respectively, $m_e = \rho_e h_e$ is the mass per unit area of the plate.
 165 In Eq. (4), following the previous assumptions on elastic plates^{16, 23}, the structural damping of the
 166 plate has not been considered. When doing so, an extra damping term may need to be involved in

This is the author's peer reviewed, accepted manuscript. However, the online version of record will be different from this version once it has been copyedited and typeset.

PLEASE CITE THIS ARTICLE AS DOI: 10.1063/1.50198106

167 Eq. (4), and the Green function used in the current scheme may need to be re-derived.

168 On the flat seabed, the impermeable boundary condition should be enforced as

$$169 \quad \frac{\partial \phi}{\partial z} = 0, \quad z = -H. \quad (5)$$

170 At the side edges of the entire system of floating elastic plates, two different conditions are
 171 considered, namely, the free edge and pinned edge conditions. The free edge conditions require zero
 172 Kirchhoff's shear force and bending moment. The pinned edge conditions require zero deflection
 173 and bending moment, which can be used to model the edge of the plate is completely moored to the
 174 seabed. Based on the above discussion, we have

$$175 \quad \begin{cases} \frac{\partial^3 \phi}{\partial x^2 \partial z} = 0, & \frac{\partial^4 \phi}{\partial x^3 \partial z} = 0 & \text{Free edge} \\ \frac{\partial \phi}{\partial z} = 0, & \frac{\partial^3 \phi}{\partial x^2 \partial z} = 0 & \text{Pinned edge} \end{cases}, \quad x = -d^+ \text{ and } x = d^-, \quad z = 0. \quad (6a, b)$$

176 In addition to the conditions at two side edges of the plates, edge conditions may also be applied to
 177 the internal constraints. The internal pins are used to model extra moored points of the elastic plate
 178 in addition to these at two sides, where the deflection is zero, the slope and bending moment are
 179 continuous, or

$$180 \quad \begin{cases} \left(\frac{\partial \phi}{\partial z} \right)_{x=a_i} = 0 \\ \left(\frac{\partial^2 \phi}{\partial x \partial z} \right)_{x=a_i^-} = \left(\frac{\partial^2 \phi}{\partial x \partial z} \right)_{x=a_i^+}, & i = 1 \sim N_a. \\ \left(\frac{\partial^3 \phi}{\partial x^2 \partial z} \right)_{x=a_i^-} = \left(\frac{\partial^3 \phi}{\partial x^2 \partial z} \right)_{x=a_i^+} \end{cases} \quad (7a, b, c)$$

181 At the location when two sides of the plate are hinged to each other, the bending moment here should
 182 be zero, as well as the deflection and shear force are continuous, or

$$183 \quad \begin{cases} \left(\frac{\partial \phi}{\partial z} \right)_{x=b_i^-} = \left(\frac{\partial \phi}{\partial z} \right)_{x=b_i^+} \\ \left(\frac{\partial^3 \phi}{\partial x^2 \partial z} \right)_{x=b_i} = 0 & , \quad i = 1 \sim N_b. \\ \left(\frac{\partial^4 \phi}{\partial x^3 \partial z} \right)_{x=b_i^-} = \left(\frac{\partial^4 \phi}{\partial x^3 \partial z} \right)_{x=b_i^+} \end{cases} \quad (8a, b, c)$$

184 For internal free edges, we have

$$185 \quad \begin{cases} \left(\frac{\partial^3 \phi}{\partial x^2 \partial z} \right)_{x=c_i} = 0 \\ \left(\frac{\partial^4 \phi}{\partial x^3 \partial z} \right)_{x=c_i} = 0 \end{cases}, \quad i = 1 \sim N_c. \quad (9a, b)$$

186 The far-field radiation conditions should be imposed at infinity to ensure wave propagating
 187 outwards, which gives

$$188 \quad \lim_{x \rightarrow \pm\infty} \left(\frac{\partial \phi_D}{\partial x} \pm i k_0 \phi_D \right) = 0, \quad (10)$$

189 where k_0 is the wavenumber of the propagation wave, which will be discussed later.

190

191 III. SOLUTION PROCEDURE

192 The method of domain decomposition is used to derive the solution. As discussed in Sec. II, there
 193 is a total of $N_a + N_b + N_c + 2$ edges in the floating solar panels shown in Fig. 1. The entire fluid
 194 domain here is only divided into three parts, where two subdomains with the free surface or Ω_1
 195 ($-\infty < x < -d, -H \leq z \leq 0$) and Ω_3 ($d < x < +\infty, -H \leq z \leq 0$), as well as the subdomain
 196 below the entire elastic plates or Ω_2 ($-d \leq x \leq d, -H \leq z \leq 0$). The velocity potential in each
 197 subdomain Ω_i ($i = 1, 2, 3$) is denoted as $\phi^{(i)}$. $\phi^{(1)}$ and $\phi^{(3)}$ can be expanded into a series of
 198 eigenfunctions, while $\phi^{(2)}$ can be constructed by using the boundary integral equation.

199 Based on the above discussion, $\phi^{(1)}$ may be written as

$$200 \quad \phi^{(1)}(x, z) = \phi_I(x, z) + \phi_D^{(1)}(x, z), \quad (11)$$

201 where the incident velocity potential $\phi_I(x, z)$ can be expressed as

$$202 \quad \phi_I(x, z) = I\varphi_0(z)e^{-ik_0x}, \quad (12)$$

203 where $I = -i\frac{Ag}{\omega}$. A denotes the amplitude of the incident wave, k_0 denotes the wave number along
 204 the x -direction and $\varphi_0(z)$ is a mode function corresponding to k_0 . Based on the far-field radiation
 205 condition Eq. (10), $\phi_D^{(1)}(x, z)$ can be expanded in the following series form as

$$206 \quad \phi_D^{(1)}(x, z) = \sum_{m=0}^{+\infty} A_m \varphi_m(z) e^{ik_m x}, \quad (13)$$

207 where A_m ($m = 0, 1, 2, \dots$) are unknown coefficients, as well as

$$208 \quad \varphi_m(z) = \frac{\cosh k_m(z+H)}{\cosh k_m H}, \quad m = 0, 1, 2, \dots, \quad (14)$$

209 with k_m satisfy the following dispersion equation of free surface wave

$$210 \quad K_1(k_m, \omega) \equiv k_m \tanh k_m - \frac{\omega^2}{g} = 0. \quad (15)$$

211 Here, k_0 is the positive real root, and k_m ($m = 1, 2, 3, \dots$) are an infinite number of purely negative
 212 imaginary roots.

213 The velocity potential $\phi^{(3)}$ in Ω_3 can be also treated in this way, which provides

$$214 \quad \phi^{(3)}(x, z) = \sum_{m=0}^{+\infty} B_m \varphi_m(z) e^{-ik_m x}, \quad (16)$$

215 where B_m ($m = 0, 1, 2, \dots$) are unknown coefficients. Due to the internal constraints in the floating
 216 elastic plates, the velocity potential $\phi^{(2)}$ in Ω_2 cannot simply be written as a series of eigenfunctions.

217 Alternatively, we may use the Green function method to construct $\phi^{(2)}$ here. To do that, the Green

This is the author's peer reviewed, accepted manuscript. However, the online version of record will be different from this version once it has been copyedited and typeset.

PLEASE CITE THIS ARTICLE AS DOI: 10.1063/1.50198106

218 function G corresponding to the water surface fully covered by a homogeneous elastic plate is first
 219 introduced²⁴

$$220 \quad G(x, z; x_0, z_0) = \ln\left(\frac{r_1}{H}\right) + \ln\left(\frac{r_2}{H}\right) - 2 \int_0^{+\infty} \frac{e^{-\alpha H}}{\alpha} \left[\frac{P(\alpha)Z(\alpha, z)Z(\alpha, z_0) \cos \alpha(x-x_0)}{K_2(\alpha, \omega)Z(\alpha, 0)} + 1 \right] d\alpha. \quad (17)$$

221 where

$$222 \quad \begin{cases} P(\alpha) = (L\alpha^4 + \rho g - m_e \omega^2)\alpha + \rho \omega^2 \\ K_2(\alpha, \omega) = (L\alpha^4 + \rho g - m_e \omega^2)\alpha \sinh \alpha H - \rho \omega^2 \cosh \alpha H. \\ Z(\alpha, z) = \cosh \alpha(z + H) \end{cases} \quad (18a, b, c)$$

223 r_1 is the distance between the field point (x, z) and source point (x_0, z_0) , and r_2 is the distance
 224 between the field point (x, z) and point $(x_0, -z_0 - 2H)$. G in Eq. (17) can be also converted into a
 225 series form, we may first extend the integral range from $(0, +\infty)$ to $(-\infty, +\infty)$, and then apply the
 226 theorem of residue, through some algebra, we have

$$227 \quad G(x, z; x_0, z_0) = \pi i \sum_{m=-2}^{+\infty} \frac{\psi_m(z)\psi_m(z_0)}{\kappa_m Q_m} e^{-i\kappa_m |x-x_0|}, \quad (19)$$

228 where

$$229 \quad Q_m = \frac{2\kappa_m H + \sinh(2\kappa_m H)}{4\kappa_m \cosh^2(\kappa_m H)} + \frac{2L\kappa_m^4}{\rho \omega^2} \tanh^2(\kappa_m H), \quad (20)$$

$$230 \quad \psi_m(z) = \frac{\cosh \kappa_m(z+H)}{\cosh \kappa_m H}, \quad m = -2, -1, 0, \dots \quad (21)$$

231 κ_m are the roots of the dispersion equation corresponding to the fluid fully covered by an elastic
 232 plate, or $K_2(\kappa_m, \omega) = 0$. κ_{-2} and κ_{-1} are two fully complex roots with negative imaginary parts
 233 and satisfy $\bar{\kappa}_{-1} = -\kappa_{-2}$, κ_0 is the purely positive real root, κ_m ($m = 1, 2, 3, \dots$) are an infinite
 234 number of purely negative imaginary roots.

235

236 As G is symmetrical about coordinates (x, z) and (x_0, z_0) , we may exchange (x, z) with (x_0, z_0)
 237 below. Applying the Green's second identity, $\phi^{(2)}(x, z)$ can be written as

$$238 \quad 2\pi\phi^{(2)}(x, z) = \oint_{\mathcal{L}} \left[\phi^{(2)}(x_0, z_0) \frac{\partial G(x, z; x_0, z_0)}{\partial n_0} - G(x, z; x_0, z_0) \frac{\partial \phi^{(2)}(x_0, z_0)}{\partial n_0} \right] dS_0, \quad (22)$$

239 where \mathcal{L} is comprised of lines $x_0 = -d, z_0 = 0, x_0 = d$ and $z_0 = -H$, $\partial/\partial n_0$ denotes the normal
 240 derivative with respect to (x_0, z_0) along \mathcal{L} . Since both G and $\phi^{(2)}$ satisfy the boundary conditions
 241 on the seabed, Eq. (22) can be further written as

$$242 \quad 2\pi\phi^{(2)}(x, z) = \left\{ \begin{aligned} & \int_{-d}^d \left[\phi^{(2)}(x_0, 0) \frac{\partial G(x, z; x_0, 0)}{\partial z_0} - G(x, z; x_0, 0) \frac{\partial \phi^{(2)}(x_0, 0)}{\partial z_0} \right] dx_0 \\ & - \int_{-H}^0 \left[\phi^{(2)}(-d, z_0) \frac{\partial G(x, z; -d, z_0)}{\partial x_0} - G(x, z; -d, z_0) \frac{\partial \phi^{(2)}(-d, z_0)}{\partial x_0} \right] dz_0 \\ & + \int_{-H}^0 \left[\phi^{(2)}(d, z_0) \frac{\partial G(x, z; d, z_0)}{\partial x_0} - G(x, z; d, z_0) \frac{\partial \phi^{(2)}(d, z_0)}{\partial x_0} \right] dz_0 \end{aligned} \right\}. \quad (23)$$

This is the author's peer reviewed, accepted manuscript. However, the online version of record will be different from this version once it has been copyedited and typeset.

PLEASE CITE THIS ARTICLE AS DOI: 10.1063/1.50198106

243 Applying the boundary condition on the elastic plate in Eq. (4) to the first integral on the right-hand
 244 side of Eq. (23), as well as using integration by parts, as in Yang, *et al.*²¹, we obtain

$$\begin{aligned}
 245 \quad & \int_{-d}^d \left[\phi^{(2)}(x_0, 0) \frac{\partial G(x, z; x_0, 0)}{\partial z_0} - G(x, z; x_0, 0) \frac{\partial \phi^{(2)}(x_0, 0)}{\partial z_0} \right] dx_0 = \\
 246 \quad & \frac{L}{\rho \omega^2} \left\{ \begin{aligned}
 & \sum_{i=1}^{N_a} \left(\frac{\partial^4 \phi^{(2)}}{\partial x_0^3 \partial z_0} \frac{\partial G}{\partial z_0} - \frac{\partial^4 G}{\partial x_0^3 \partial z_0} \frac{\partial \phi^{(2)}}{\partial z_0} - \frac{\partial^3 \phi^{(2)}}{\partial x_0^2 \partial z_0} \frac{\partial^2 G}{\partial x_0 \partial z_0} + \frac{\partial^3 G}{\partial x_0^2 \partial z_0} \frac{\partial^2 \phi^{(2)}}{\partial x_0 \partial z_0} \right)_{x_0=a_i^+}^{x_0=a_i^-} \\
 & + \sum_{i=1}^{N_b} \left(\frac{\partial^4 \phi^{(2)}}{\partial x_0^3 \partial z_0} \frac{\partial G}{\partial z_0} - \frac{\partial^4 G}{\partial x_0^3 \partial z_0} \frac{\partial \phi^{(2)}}{\partial z_0} - \frac{\partial^3 \phi^{(2)}}{\partial x_0^2 \partial z_0} \frac{\partial^2 G}{\partial x_0 \partial z_0} + \frac{\partial^3 G}{\partial x_0^2 \partial z_0} \frac{\partial^2 \phi^{(2)}}{\partial x_0 \partial z_0} \right)_{x_0=b_i^+}^{x_0=b_i^-} \\
 & + \sum_{i=1}^{N_c} \left(\frac{\partial^4 \phi^{(2)}}{\partial x_0^3 \partial z_0} \frac{\partial G}{\partial z_0} - \frac{\partial^4 G}{\partial x_0^3 \partial z_0} \frac{\partial \phi^{(2)}}{\partial z_0} - \frac{\partial^3 \phi^{(2)}}{\partial x_0^2 \partial z_0} \frac{\partial^2 G}{\partial x_0 \partial z_0} + \frac{\partial^3 G}{\partial x_0^2 \partial z_0} \frac{\partial^2 \phi^{(2)}}{\partial x_0 \partial z_0} \right)_{x_0=c_i^+}^{x_0=c_i^-} \\
 & + \left(\frac{\partial^4 \phi^{(2)}}{\partial x_0^3 \partial z_0} \frac{\partial G}{\partial z_0} - \frac{\partial^4 G}{\partial x_0^3 \partial z_0} \frac{\partial \phi^{(2)}}{\partial z_0} - \frac{\partial^3 \phi^{(2)}}{\partial x_0^2 \partial z_0} \frac{\partial^2 G}{\partial x_0 \partial z_0} + \frac{\partial^3 G}{\partial x_0^2 \partial z_0} \frac{\partial^2 \phi^{(2)}}{\partial x_0 \partial z_0} \right)_{x_0=-d}^{x_0=d}
 \end{aligned} \right\}. \quad (24)
 \end{aligned}$$

247 To simplify Eq. (24), we may invoke the conditions at the internal constraints. Using Eqs. (7), (8)

248 and (9), we have $\left(\frac{\partial \phi^{(2)}}{\partial z_0} \right)_{x_0=a_i^+}^{x_0=a_i^-} = \left(\frac{\partial^2 \phi^{(2)}}{\partial x_0 \partial z_0} \right)_{x_0=a_i^+}^{x_0=a_i^-} = \left(\frac{\partial^3 \phi^{(2)}}{\partial x_0^2 \partial z_0} \right)_{x_0=a_i^+}^{x_0=a_i^-} = 0$, which means there is no

249 jump in the deflection, slope and bending moment. $\left(\frac{\partial \phi^{(2)}}{\partial z_0} \right)_{x_0=b_i^+}^{x_0=b_i^-} = \left(\frac{\partial^3 \phi^{(2)}}{\partial x_0^2 \partial z_0} \right)_{x_0=b_i^+}^{x_0=b_i^-} =$

250 $\left(\frac{\partial^4 \phi^{(2)}}{\partial x_0^3 \partial z_0} \right)_{x_0=b_i^+}^{x_0=b_i^-} = 0$, which alludes no jump in the deflection, bending moment and shear force.

251 Besides, $\left(\frac{\partial^4 \phi^{(2)}}{\partial x_0^3 \partial z_0} \right)_{x_0=c_i^+}^{x_0=c_i^-} = \left(\frac{\partial^3 \phi^{(2)}}{\partial x_0^2 \partial z_0} \right)_{x_0=c_i^+}^{x_0=c_i^-} = 0$. We may further define these jumps at a_i , b_i and c_i as

252 the following unknowns.

$$253 \quad \begin{cases} \alpha_i = \frac{L}{2\pi\rho\omega^2} \left(\frac{\partial^4 \phi^{(2)}}{\partial x_0^3 \partial z_0} \right)_{x_0=a_i^+}^{x_0=a_i^-}, & i = 1 \sim N_a \\ \beta_i = \frac{L}{2\pi\rho\omega^2} \left(\frac{\partial^2 \phi^{(2)}}{\partial x_0 \partial z_0} \right)_{x_0=b_i^+}^{x_0=b_i^-}, & i = 1 \sim N_b \\ \gamma_i = \frac{L}{2\pi\rho\omega^2} \left(-\frac{\partial \phi^{(2)}}{\partial z_0} \right)_{x_0=c_i^+}^{x_0=c_i^-}, \quad \mu_i = \frac{L}{2\pi\rho\omega^2} \left(\frac{\partial^2 \phi^{(2)}}{\partial x_0 \partial z_0} \right)_{x_0=c_i^+}^{x_0=c_i^-}, & i = 1 \sim N_c \end{cases}, \quad (25a-c)$$

254 as well as introduce

$$255 \quad \mathcal{G}(x, z, x_0) = \frac{\partial G(x, z; x_0, 0)}{\partial z_0} = \pi i \sum_{m=-2}^{+\infty} \frac{\psi_m(z) \tanh(\kappa_m H) e^{-i\kappa_m |x-x_0|}}{Q_m}. \quad (26)$$

256 In Eq. (24), we may apply the Laplace equation, or $\frac{\partial^2}{\partial x_0^2} = -\frac{\partial^2}{\partial z_0^2}$ to the terms of G and $\phi^{(2)}$ at $x_0 =$

257 $\pm d$. Together with the above discussion, Eq. (24) becomes

$$258 \quad \int_{-d}^d \left[\phi^{(2)}(x_0, 0) \frac{\partial G(x, z; x_0, 0)}{\partial z_0} - G(x, z; x_0, 0) \frac{\partial \phi^{(2)}(x_0, 0)}{\partial z_0} \right] dx_0 =$$

This is the author's peer reviewed, accepted manuscript. However, the online version of record will be different from this version once it has been copyedited and typeset.

PLEASE CITE THIS ARTICLE AS DOI: 10.1063/1.50198106

$$\left. \begin{aligned}
 & 2\pi \sum_{i=1}^{N_a} \alpha_i \mathcal{G}(x, z, a_i) + 2\pi \sum_{i=1}^{N_b} \beta_i \frac{\partial^2 \mathcal{G}(x, z, b_i)}{\partial x_0^2} \\
 & + 2\pi \sum_{i=1}^{N_c} \left[\gamma_i \frac{\partial^3 \mathcal{G}(x, z, c_i)}{\partial x_0^3} + \mu_i \frac{\partial^2 \mathcal{G}(x, z, c_i)}{\partial x_0^2} \right] \\
 & + \frac{L}{\rho \omega^2} \left(-\frac{\partial^4 \phi^{(2)}}{\partial x_0 \partial z_0^3} \frac{\partial G}{\partial z_0} + \frac{\partial^4 G}{\partial x_0 \partial z_0^2} \frac{\partial \phi^{(2)}}{\partial z_0} + \frac{\partial^3 \phi^{(2)}}{\partial z_0^3} \frac{\partial^2 G}{\partial x_0 \partial z_0} - \frac{\partial^3 G}{\partial z_0^3} \frac{\partial^2 \phi^{(2)}}{\partial x_0 \partial z_0} \right)_{x_0 = -d}^{x_0 = d}
 \end{aligned} \right\}. \quad (27)$$

Substituting Eq. (27) into (23) and using the following inner product for z_0 ²⁵

$$\langle f, g \rangle = \int_{-H}^0 f g d z_0 + \frac{L}{\rho \omega^2} \left(\frac{d^3 f}{d z^3} \frac{d g}{d z} + \frac{d f}{d z} \frac{d^3 g}{d z^3} \right)_{z_0=0} \quad (28)$$

We have

$$\begin{aligned}
 \phi^{(2)}(x, z) = & \frac{1}{2\pi} \left\{ \left\langle \frac{\partial \mathcal{G}(x, z; d, z_0)}{\partial x_0}, \phi^{(2)}(d, z_0) \right\rangle - \left\langle G(x, z; d, z_0), \frac{\partial \phi^{(2)}(d, z_0)}{\partial x_0} \right\rangle \right. \\
 & \left. + \left\langle G(x, z; -d, z_0), \frac{\partial \phi^{(2)}(-d, z_0)}{\partial x_0} \right\rangle - \left\langle \frac{\partial \mathcal{G}(x, z; -d, z_0)}{\partial x_0}, \phi^{(2)}(-d, z_0) \right\rangle \right\} + \\
 & \left\{ \sum_{i=1}^{N_a} \alpha_i \mathcal{G}(x, z, a_i) + \sum_{i=1}^{N_b} \beta_i \frac{\partial^2 \mathcal{G}(x, z, b_i)}{\partial x_0^2} \right. \\
 & \left. + \sum_{i=1}^{N_c} \left[\gamma_i \frac{\partial^3 \mathcal{G}(x, z, c_i)}{\partial x_0^3} + \mu_i \frac{\partial^2 \mathcal{G}(x, z, c_i)}{\partial x_0^2} \right] \right\}, \quad |x| < d. \quad (29)
 \end{aligned}$$

Based on the derivation in Yang, *et al.*²⁶, the terms at $x_0 = \pm d$ in Eq. (29) are equivalent to be written via a source distribution formula, which gives

$$\begin{aligned}
 \phi^{(2)}(x, z) = & \langle G(x, z; d, z_0), \Psi_+(z_0) \rangle - \langle G(x, z; -d, z_0), \Psi_-(z_0) \rangle + \\
 & \left\{ \sum_{i=1}^{N_a} \alpha_i \mathcal{G}(x, z, a_i) + \sum_{i=1}^{N_b} \beta_i \frac{\partial^2 \mathcal{G}(x, z, b_i)}{\partial x_0^2} \right. \\
 & \left. + \sum_{i=1}^{N_c} \left[\gamma_i \frac{\partial^3 \mathcal{G}(x, z, c_i)}{\partial x_0^3} + \mu_i \frac{\partial^2 \mathcal{G}(x, z, c_i)}{\partial x_0^2} \right] \right\}, \quad |x| < d, \quad (30)
 \end{aligned}$$

where $\Psi_{\pm}(z_0)$ are the source strengths along the lines $x_0 = \pm d$ respectively. We may expand $\Psi_{\pm}(z_0)$ as the following series of eigenfunctions

$$\begin{cases} \Psi_+(z_0) = \frac{1}{\pi i} \sum_{m=-2}^{+\infty} \kappa_m e^{i\kappa_m d} C_m \psi_m(z) \\ \Psi_-(z_0) = \frac{1}{\pi i} \sum_{m=-2}^{+\infty} \kappa_m e^{i\kappa_m d} D_m \psi_m(z) \end{cases} \quad (31a, b)$$

where C_m and D_m are unknown coefficients. Substituting Eqs. (19) and (31) into Eq. (30), as well as invoking the orthogonality of inner product $\langle \psi_m(z_0), \psi_{\bar{m}}(z_0) \rangle = \delta_{m\bar{m}} Q_m$, where $\delta_{m\bar{m}}$ denotes the Kronecker delta function, which gives

$$\begin{aligned}
 \phi^{(2)}(x, z) = & \sum_{m=-2}^{+\infty} (C_m e^{-i\kappa_m x} + D_m e^{i\kappa_m x}) \psi_m(z) + \\
 & \left\{ \sum_{i=1}^{N_a} \alpha_i \mathcal{G}(x, z, a_i) + \sum_{i=1}^{N_b} \beta_i \frac{\partial^2 \mathcal{G}(x, z, b_i)}{\partial x_0^2} \right. \\
 & \left. + \sum_{i=1}^{N_c} \left[\gamma_i \frac{\partial^3 \mathcal{G}(x, z, c_i)}{\partial x_0^3} + \mu_i \frac{\partial^2 \mathcal{G}(x, z, c_i)}{\partial x_0^2} \right] \right\}, \quad |x| < d. \quad (32)
 \end{aligned}$$

282 To solve the unknown coefficients $A_m, B_m, C_m, D_m, \alpha_i, \beta_i, \gamma_i$ and μ_i , we may use the continuous
 283 conditions of the velocity potential and dynamic pressure at two interfaces $x = \pm d$, or

$$284 \begin{cases} \phi^{(1)}(-d^-, z) = \phi^{(2)}(-d^+, z) \\ \frac{\partial \phi^{(1)}(-d^-, z)}{\partial x} = \frac{\partial \phi^{(2)}(-d^+, z)}{\partial x} \\ \phi^{(2)}(d^-, z) = \phi^{(3)}(d^+, z) \\ \frac{\partial \phi^{(2)}(d^-, z)}{\partial x} = \frac{\partial \phi^{(3)}(d^+, z)}{\partial x} \end{cases} \quad (33a-d)$$

285 To match the velocity potentials at $x = \pm d$, from Eqs. (33a) and (33c), we have

$$286 \begin{cases} \int_{-H}^0 \phi^{(1)}(-d, z) \varphi_m(z) dz = \int_{-H}^0 \phi^{(2)}(-d, z) \varphi_m(z) dz \\ \int_{-H}^0 \phi^{(3)}(d, z) \varphi_m(z) dz = \int_{-H}^0 \phi^{(2)}(d, z) \varphi_m(z) dz \end{cases} \quad (34a, b)$$

287 Substituting Eqs. (11), (12), (13), (16) and (32) into Eqs. (34a) and (34b), as well as using the
 288 orthogonality of $\varphi_m(z)$, which gives the following system of linear equations

$$289 \begin{aligned} & P_m e^{-i\ell_m d} A_m - \sum_{m'=-2}^{+\infty} X(\kappa_{m'}, \ell_m) (e^{i\kappa_{m'} d} C_{m'} + e^{-i\kappa_{m'} d} D_{m'}) - \\ & \left\{ \sum_{i=1}^{N_a} \mathcal{F}_m(-d, \alpha_i) \alpha_i + \sum_{i=1}^{N_b} \frac{\partial^2 \mathcal{F}_m(-d, b_i)}{\partial x_0^2} \beta_i \right\} \\ & \left. + \sum_{i=1}^{N_c} \left[\frac{\partial^3 \mathcal{F}_m(-d, c_i)}{\partial x_0^3} \gamma_i + \frac{\partial^2 \mathcal{F}_m(-d, c_i)}{\partial x_0^2} \mu_i \right] \right\} = -\delta_{m0} I P_0 e^{i\ell_0 d}, \quad m = 0, 1, 2, \dots, \end{aligned} \quad (35a)$$

$$292 \begin{aligned} & P_m e^{-i\ell_m d} B_m - \sum_{m'=-2}^{+\infty} X(\kappa_{m'}, \ell_m) (e^{-i\kappa_{m'} d} C_{m'} + e^{i\kappa_{m'} d} D_{m'}) - \\ & \left\{ \sum_{i=1}^{N_a} \mathcal{F}_m(d, \alpha_i) \alpha_i + \sum_{i=1}^{N_b} \frac{\partial^2 \mathcal{F}_m(d, b_i)}{\partial x_0^2} \beta_i \right\} \\ & \left. + \sum_{i=1}^{N_c} \left[\frac{\partial^3 \mathcal{F}_m(d, c_i)}{\partial x_0^3} \gamma_i + \frac{\partial^2 \mathcal{F}_m(d, c_i)}{\partial x_0^2} \mu_i \right] \right\} = 0, \quad m = 0, 1, 2, \dots, \end{aligned} \quad (35b)$$

293 where

$$294 \begin{cases} X(x_1, x_2) = \int_{-H}^0 \frac{\cosh x_1(z+H) \cosh x_2(z+H)}{\cosh x_1 H \cosh x_2 H} dz = \begin{cases} \frac{x_1 \tanh x_1 H - x_2 \tanh x_2 H}{x_1^2 - x_2^2} & x_1 \neq x_2 \\ \frac{\sinh 2x_1 H + 2x_1 H}{4x_1 \cosh^2 x_1 H} & x_1 = x_2 \end{cases} \\ P_m = X(\ell_m, \ell_m) = \frac{2\ell_m H + \sinh(2\ell_m H)}{4\ell_m \cosh^2(\ell_m H)} \\ \mathcal{F}_m(x, x_0) = \int_{-H}^0 \mathcal{G}(x, z, x_0) \varphi_m(z) dz = \pi i \sum_{m'=-2}^{+\infty} \frac{X(\kappa_{m'}, \ell_m) \tanh(\kappa_{m'} H) e^{-i\kappa_{m'} |x-x_0|}}{Q_{m'}} \end{cases} \quad (36a, b, c)$$

295 To match the velocity at $x = \pm d$, we may apply

$$296 \left\langle \frac{\partial \phi^{(2)}(\pm d, z)}{\partial x}, \psi_m(z) \right\rangle = \int_{-H}^0 \frac{\partial \phi^{(2)}(\pm d, z)}{\partial x} \psi_m(z) dz + \frac{L}{\rho \omega^2} \left[\frac{\partial^2 \phi^{(2)}(\pm d, 0)}{\partial x \partial z} \frac{d^3 \psi_m(0)}{dz^3} + \frac{\partial^4 \phi^{(2)}(\pm d, 0)}{\partial x \partial z^2} \frac{d \psi_m(0)}{dz} \right]. \quad (37)$$

297 Eqs. (33b) and (33d) gives

$$301 \begin{cases} \left\langle \frac{\partial \phi^{(2)}(-d, z)}{\partial x}, \psi_m(z) \right\rangle = \int_{-H}^0 \frac{\partial \phi^{(1)}(-d, z)}{\partial x} \psi_m(z) dz + \frac{L}{\rho \omega^2} \left[\frac{\partial^2 \phi^{(2)}(-d, 0)}{\partial x \partial z} \frac{d^3 \psi_m(0)}{dz^3} + \frac{\partial^4 \phi^{(2)}(-d, 0)}{\partial x \partial z^2} \frac{d \psi_m(0)}{dz} \right] \\ \left\langle \frac{\partial \phi^{(2)}(d, z)}{\partial x}, \psi_m(z) \right\rangle = \int_{-H}^0 \frac{\partial \phi^{(3)}(d, z)}{\partial x} \psi_m(z) dz + \frac{L}{\rho \omega^2} \left[\frac{\partial^2 \phi^{(2)}(d, 0)}{\partial x \partial z} \frac{d^3 \psi_m(0)}{dz^3} + \frac{\partial^4 \phi^{(2)}(d, 0)}{\partial x \partial z^2} \frac{d \psi_m(0)}{dz} \right] \end{cases}$$

This is the author's peer reviewed, accepted manuscript. However, the online version of record will be different from this version once it has been copyedited and typeset.

PLEASE CITE THIS ARTICLE AS DOI: 10.1063/1.50198106

302 (38a, b)

303 We may further define

$$304 \quad \begin{cases} \frac{\partial^2 \phi^{(2)}(\pm d, 0)}{\partial x \partial z} = \zeta_{\pm} \\ \frac{\partial^4 \phi^{(2)}(\pm d, 0)}{\partial x \partial z^3} = \xi_{\pm} \end{cases}, \quad (39a, b)$$

305 where ζ_{\pm} and ξ_{\pm} are introduced as additional unknowns to satisfy the edge conditions at $x = \pm d$
 306 later. Substituting Eqs. (11), (12), (13), (16) and (32) into Eqs. (38a) and (38b), as well as using the
 307 orthogonality of $\psi_m(z)$, which provides

$$308 \quad -i \sum_{m'=0}^{+\infty} X(\kappa_m, \ell_{m'}) \ell_{m'} e^{-i\ell_{m'} d} A_{m'} + i\kappa_m Q_m (-e^{i\kappa_m d} C_m + e^{-i\kappa_m d} D_m) + \\ 309 \quad \left\{ \sum_{i=1}^{N_a} \frac{\partial g_m(-d, a_i)}{\partial x} \alpha_i + \sum_{i=1}^{N_b} \frac{\partial^2 g_m(-d, b_i)}{\partial x \partial x_0^2} \beta_i \right\} + \kappa_m \tanh(\kappa_m H) (\kappa_m^2 \zeta_- + \xi_-) = \\ 310 \quad -iX(\kappa_m, \ell_0) \ell_0 e^{i\ell_0 d}, \quad m = -2, -1, 0, 1, \dots, \quad (40a)$$

$$312 \quad i \sum_{m'=0}^{+\infty} X(\kappa_m, \ell_{m'}) \ell_{m'} e^{-i\ell_{m'} d} B_{m'} + i\kappa_m Q_m (-e^{-i\kappa_m d} C_m + e^{i\kappa_m d} D_m) + \\ 313 \quad \left\{ \sum_{i=1}^{N_a} \frac{\partial g_m(d, a_i)}{\partial x} \alpha_i + \sum_{i=1}^{N_b} \frac{\partial^2 g_m(d, b_i)}{\partial x \partial x_0^2} \beta_i \right\} + \kappa_m \tanh(\kappa_m H) (\kappa_m^2 \zeta_+ + \xi_+) = 0, \quad m = -2, -1, 0, \dots, \\ 314 \quad (40b)$$

315 where

$$316 \quad g_m(x, x_0) = \langle \mathcal{G}(x, z, x_0), \psi_m(z) \rangle = \pi i \tanh(\kappa_m H) e^{-i\kappa_m |x - x_0|}. \quad (41)$$

317 The remaining equations can be established from the edge conditions at $x = a_j, b_j, c_j$ and $x = \pm d$.

318 In particular, applying Eq. (7a) to Eq. (32), the edge condition at $x = a_j$ ($j = 1 \sim N_a$) gives

$$319 \quad \sum_{m'=-2}^{+\infty} [f_m^-(a_j) C_{m'} + f_m^+(a_j) D_{m'}] + \left\{ \sum_{i=1}^{N_a} \mathcal{W}(a_j, a_i) \alpha_i + \sum_{i=1}^{N_b} \frac{\partial^2 \mathcal{W}(a_j, b_i)}{\partial x_0^2} \beta_i \right\} + \\ \left\{ + \sum_{i=1}^{N_c} \left[\frac{\partial^3 \mathcal{W}(a_j, c_i)}{\partial x_0^3} \gamma_i + \frac{\partial^2 \mathcal{W}(a_j, c_i)}{\partial x_0^2} \mu_i \right] \right\} = 0, \quad (42)$$

320 where

$$321 \quad \begin{cases} f_m^{\pm}(x) = \kappa_m \tanh(\kappa_m H) e^{\pm i\kappa_m x} \\ \mathcal{W}(x, x_0) = \frac{\partial \mathcal{G}(x, 0, x_0)}{\partial z} = \pi i \sum_{m=-2}^{+\infty} \frac{\kappa_m \tanh^2(\kappa_m H) e^{-i\kappa_m |x - x_0|}}{Q_m} \end{cases} \quad (43a, b)$$

322 Applying Eq. (8b) to Eq. (32), the edge condition at $x = b_j$ ($j = 1 \sim N_b$) gives

$$323 \quad \sum_{m'=-2}^{+\infty} \left[\frac{d^2 f_m^-(b_j)}{dx^2} C_{m'} + \frac{d^2 f_m^+(b_j)}{dx^2} D_{m'} \right] + \left\{ \sum_{i=1}^{N_a} \frac{\partial^2 \mathcal{W}(b_j, a_i)}{\partial x^2} \alpha_i + \sum_{i=1}^{N_b} \frac{\partial^4 \mathcal{W}(b_j, b_i)}{\partial x^2 \partial x_0^2} \beta_i \right\} + \\ \left\{ + \sum_{i=1}^{N_c} \left[\frac{\partial^5 \mathcal{W}(b_j, c_i)}{\partial x^2 \partial x_0^3} \gamma_i + \frac{\partial^4 \mathcal{W}(b_j, c_i)}{\partial x^2 \partial x_0^2} \mu_i \right] \right\} = 0. \quad (44)$$

324 Using Eqs. (9a, b) to Eq. (32), the edge condition at $x = c_j$ ($j = 1 \sim N_b$) gives

This is the author's peer reviewed, accepted manuscript. However, the online version of record will be different from this version once it has been copyedited and typeset.

PLEASE CITE THIS ARTICLE AS DOI: 10.1063/1.50198106

$$325 \quad \sum_{m'=-2}^{+\infty} \left[\frac{d^2 f_m^-(c_j)}{dx^2} C_{m'} + \frac{d^2 f_m^+(c_j)}{dx^2} D_{m'} \right] + \left\{ \begin{array}{l} \sum_{i=1}^{N_a} \frac{\partial^2 \mathcal{W}(c_j, a_i)}{\partial x^2} \alpha_i + \sum_{i=1}^{N_b} \frac{\partial^4 \mathcal{W}(c_j, b_i)}{\partial x^2 \partial x_0^2} \beta_i \\ + \sum_{i=1}^{N_c} \left[\frac{\partial^5 \mathcal{W}(c_j, c_i)}{\partial x^2 \partial x_0^3} \gamma_i + \frac{\partial^4 \mathcal{W}(c_j, c_i)}{\partial x^2 \partial x_0^2} \mu_i \right] \end{array} \right\} = 0, \quad (45a)$$

$$326 \quad \sum_{m'=-2}^{+\infty} \left[\frac{d^3 f_m^-(c_j)}{dx^3} C_{m'} + \frac{d^3 f_m^+(c_j)}{dx^3} D_{m'} \right] + \left\{ \begin{array}{l} \sum_{i=1}^{N_a} \frac{\partial^3 \mathcal{W}(c_j, a_i)}{\partial x^3} \alpha_i + \sum_{i=1}^{N_b} \frac{\partial^5 \mathcal{W}(b_j, b_i)}{\partial x^3 \partial x_0^2} \beta_i \\ + \sum_{i=1}^{N_c} \left[\frac{\partial^6 \mathcal{W}(c_j, c_i)}{\partial x^3 \partial x_0^3} \gamma_i + \frac{\partial^5 \mathcal{W}(c_j, c_i)}{\partial x^3 \partial x_0^2} \mu_i \right] \end{array} \right\} = 0. \quad (45b)$$

327 If the edges at $x = \pm d$ are free to move, substituting Eq. (32) into Eq. (6a), similar equations shown
328 in Eqs. (45a, b) need to be satisfied, or

$$329 \quad \sum_{m'=-2}^{+\infty} \left[\frac{d^2 f_m^-(\pm d)}{dx^2} C_{m'} + \frac{d^2 f_m^+(\pm d)}{dx^2} D_{m'} \right] + \left\{ \begin{array}{l} \sum_{i=1}^{N_a} \frac{\partial^2 \mathcal{W}(\pm d, a_i)}{\partial x^2} \alpha_i + \sum_{i=1}^{N_b} \frac{\partial^4 \mathcal{W}(\pm d, b_i)}{\partial x^2 \partial x_0^2} \beta_i \\ \sum_{i=1}^{N_c} \left[\frac{\partial^5 \mathcal{W}(\pm d, c_i)}{\partial x^2 \partial x_0^3} \gamma_i + \frac{\partial^4 \mathcal{W}(\pm d, c_i)}{\partial x^2 \partial x_0^2} \mu_i \right] \end{array} \right\} = 0, \quad (46a)$$

$$330 \quad \sum_{m'=-2}^{+\infty} \left[\frac{d^3 f_m^-(\pm d)}{dx^3} C_{m'} + \frac{d^3 f_m^+(\pm d)}{dx^3} D_{m'} \right] + \left\{ \begin{array}{l} \sum_{i=1}^{N_a} \frac{\partial^3 \mathcal{W}(\pm d, a_i)}{\partial x^3} \alpha_i + \sum_{i=1}^{N_b} \frac{\partial^5 \mathcal{W}(\pm d, b_i)}{\partial x^3 \partial x_0^2} \beta_i \\ \sum_{i=1}^{N_c} \left[\frac{\partial^6 \mathcal{W}(c_j, c_i)}{\partial x^3 \partial x_0^3} \gamma_i + \frac{\partial^5 \mathcal{W}(\pm d, c_i)}{\partial x^3 \partial x_0^2} \mu_i \right] \end{array} \right\} = 0. \quad (46b)$$

331 By contrast, if the edges at $x = \pm d$ are pinned to the seabed, the zero-shear force condition in Eq.
332 (46b) should be replaced by the zero-deflection condition as

$$333 \quad \sum_{m'=-2}^{+\infty} [f_m^-(\pm d) C_{m'} + f_m^+(\pm d) D_{m'}] + \left\{ \begin{array}{l} \sum_{i=1}^{N_a} \mathcal{W}(\pm d, a_i) \alpha_i + \sum_{i=1}^{N_b} \frac{\partial^2 \mathcal{W}(\pm d, b_i)}{\partial x_0^2} \beta_i \\ \sum_{i=1}^{N_c} \left[\frac{\partial^3 \mathcal{W}(\pm d, c_i)}{\partial x_0^3} \gamma_i + \frac{\partial^2 \mathcal{W}(\pm d, c_i)}{\partial x_0^2} \mu_i \right] \end{array} \right\} = 0. \quad (47)$$

334 If the infinite series in Eqs. (13), (16) and (31) are truncated at $m = M$, there will be $M + 1$
335 unknowns for A_m , $M + 1$ for B_m , $M + 3$ for C_m and $M + 3$ for D_m . Besides, the edge condition at
336 $x = a_i$ ($i = 1 \sim N_a$) provides N_a unknowns for α_i . The edge condition at $x = b_i$ ($i = 1 \sim N_b$) gives
337 N_b unknowns for β_i . The edge condition at $x = c_i$ ($i = 1 \sim N_c$) gives $2N_c$ unknowns for γ_i and μ_i
338 respectively. The edge conditions at $x = \pm d$ also provides 4 additional unknowns for ζ_{\pm} and ξ_{\pm}
339 respectively. In such a case, we have $4M + 12 + N_a + N_b + 2N_c$ unknowns. Eqs. (35a, b) and (40a,
340 b) provide $4M + 8$ equations, Eqs. (42), (44) ~ (47) offers $N_a + N_b + 2N_c + 4$ equations. Hence,
341 the total number of unknowns is equal to the total number of equations, and all the unknowns can
342 be fully solved. By contrast, if we employ the procedure of MEE in Ren, *et al.*¹³ instead, there will
343 be a total of $2(M + 1) + 2(N_a + N_b + N_c + 1)(M + 3)$ unknown coefficients to solve. It can be
344 found that the number of unknowns is significantly reduced by using the present method.

345

346 IV. RESULTS AND DISCUSSION

347 The typical values of physical parameters of an elastic plate are selected based on the data in Xia,
348 *et al.*²⁷,

$$349 \quad L = 1.96 \times 10^{11} \text{ N} \cdot \text{m}, \quad \rho_e = 1000 \text{ kg/m}^3, \quad h_e = 5 \text{ m}, \quad d = 150 \text{ m}. \quad (48)$$

This is the author's peer reviewed, accepted manuscript. However, the online version of record will be different from this version once it has been copyedited and typeset.

PLEASE CITE THIS ARTICLE AS DOI: 10.1063/1.50198106

350 Other parameters are chosen as $\rho = 1025 \text{ kg/m}^3$, $g = 9.81 \text{ m/s}^2$ and $H = 50 \text{ m}$. Those
 351 parameters outlined above will be applied in subsequent computations unless specified otherwise.
 352 The infinite series in Eqs. (13), (16) and (31) are truncated at $m = M = 100$, which has been
 353 confirmed to be convergent.

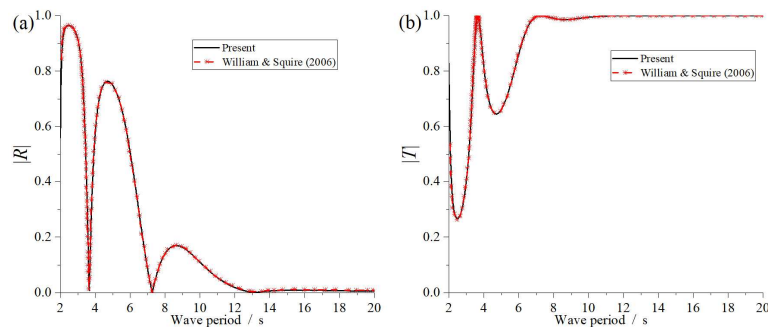
354

355 **A. Validation of the method**

356 Let $|x| \rightarrow +\infty$ in the velocity potential in Eqs. (11), (12), (13) and (16), all the decay terms will be
 357 zero, and we have

$$358 \quad \phi(x, z) = \begin{cases} I(R e^{ik_0 x} + e^{-ik_0 x})\varphi_0(z) & x \rightarrow -\infty \\ IT\varphi_0(z)e^{-ik_0 x} & x \rightarrow +\infty \end{cases}, \quad (49)$$

359 where $R = A_0/I$ and $T = B_0/I$ denote the reflection and transmission coefficients respectively. The
 360 approach applied here is validated by comparing with the results of $|R|$ and $|T|$ in [Williams and](#)
 361 [Squire¹⁰](#) for water wave diffracted by a single floating ice cover in deep water, which was solved
 362 via the Wiener-Hopf technique²⁸. $|R|$ & $|T|$ versus the wave period are plotted in Fig. 2, and a very
 363 good consistency can be observed.



364

365 Fig. 2. The reflection and transmission coefficients for an incident wave diffracted by a single
 366 floating elastic plate: (a). reflection coefficients; (b). transmission coefficients.

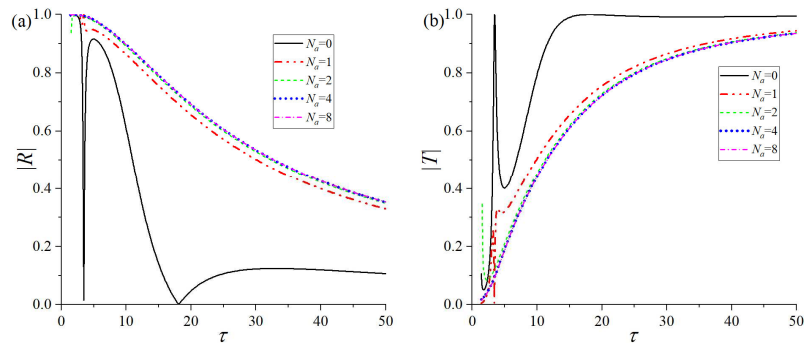
367

368 In the following sections, all the numerical results will be presented in nondimensionalized forms,
 369 based on the water density ρ , acceleration due to gravity g , and the mean water depth H . $\tau =$
 370 $\mathcal{T}\sqrt{g/H}$ is used to represent the dimensionless wave period \mathcal{T} , where $\mathcal{T} = 2\pi/\omega$. Similar with
 371 [Williams and Squire¹⁰](#), we may display the results of $\tau > 1$ here, and much attention is paid to long
 372 waves.

373

374 **B. Wave interaction with floating elastic plates with same type of internal constraints**

375 In this section, all the internal edges of the plates are considered as a single type, namely pinned,
376 hinged or free. For each type of edge, we aim to understand how the number of edges affects the
377 reflected and transmitted waves at the far-field, as well as the deflection and strain in the elastic
378 plates. Notably, the waves at infinity can be used to assess the environmental impact of deploying
379 solar panels at sea. The deflection and strain provide insights into the hydroelastic response of solar
380 panels to ocean waves.



381

382 Fig. 3. The reflection and transmission coefficients versus the wave period under different
383 numbers of internal pinned supports: (a). reflection coefficients; (b). transmission coefficients.

384

Here, two edges at $x = \pm d$ are pinned, $N_b = N_c = 0$.

385

386 **1. All internal constraints are pinned supports**

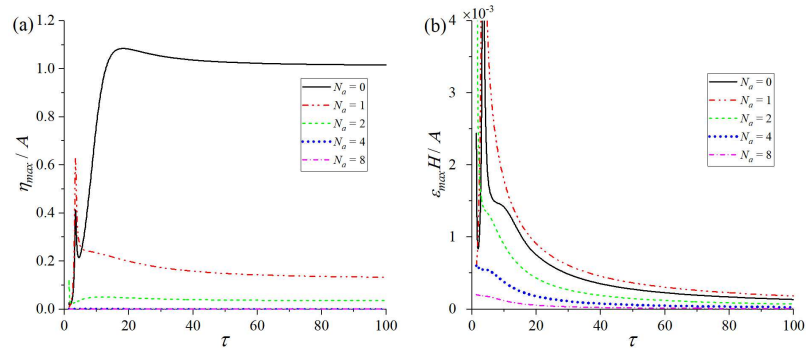
387 The pinned supports are assumed to be distributed uniformly along the plate, which gives

$$388 \quad a_i = -d + \frac{2d}{N_a+1}i, \quad i = 1 \sim N_a, \quad (50)$$

389

390 where a_i is defined in Table 1. The results of reflection and transmission coefficients are shown in
391 Fig. 3. It should be noted that when τ is small (corresponding to short waves), very highly rapid
392 changes on $|T|$ and $|R|$ are expected^{10, 16}, which is not included in the figures. On the curve of $N_a =$
393 0, T first decreases to a very small value as τ increases, and then quickly increases to a peak value
394 around $\tau \approx 4.88$. As τ continues to increase, $|R|$ decreases to a value close to 0, and then $|R|$
increases and varies much more slowly. When there is a pinned support in the elastic plate ($N_a = 1$),

395 the result becomes quite different. Specifically, $|R|$ ($|T|$) generally decreases (increases) as τ
 396 increases within the range considered in Fig. 3. Besides, at a fixed value of τ , if more pinned points
 397 are imposed on the plate, there will first be a slight increase (decrease) in $|R|$ ($|T|$). However, as N_a
 398 increases, the curves of $|R|$ ($|T|$) under $N_a = 4$ and 8 are nearly identical, which means the effect
 399 of N_a on $|R|$ ($|T|$) becomes quite weak after $N_a \geq 4$. In fact, more pinned supports in the structure
 400 means more 0-deflection points on the plate. When N_a is sufficiently large, the floating elastic plate
 401 will behave similarly to a rigid plate. Furthermore, from the aspect of wave energy, when pinned
 402 supports are imposed on the plate. For long waves, compared with the panel without any pin, the
 403 wave energy on reflected waves will increase and the on transmitted waves will decrease.



404
 405 Fig. 4. The maximum deflection and principal strain in the elastic plate versus the wave period
 406 under different numbers of internal pinned supports: (a). maximum deflection; (b) maximum
 407 principal strain. Here, two edges at $x = \pm d$ are pinned, $N_b = N_c = 0$.
 408

409 The deflection η and principal strain ε of the elastic plate are also considered, which can be
 410 calculated from²⁹

$$411 \begin{cases} \eta(x) = \frac{1}{i\omega} \frac{\partial \phi^{(2)}(x,0)}{\partial z} \\ \varepsilon(x) = \frac{h_e}{2} \left| \frac{d^2 \eta(x)}{dx^2} \right| \end{cases} \quad (51a, b)$$

412 Substituting Eq. (32) into (51a), $\eta(x)$ gives

$$413 \eta(x) = \frac{1}{i\omega} \sum_{m=-2}^{+\infty} [C_m f_m^-(x) + D_m f_m^+(x)] + \frac{1}{i\omega} \left\{ \begin{aligned} &\sum_{i=1}^{N_a} \alpha_i \mathcal{W}(x, a_i) + \sum_{i=1}^{N_b} \beta_i \frac{\partial^2 \mathcal{W}(x, b_i)}{\partial x_0^2} \\ &+ \sum_{i=1}^{N_c} [\gamma_i \frac{\partial^3 \mathcal{W}(x, c_i)}{\partial x_0^3} + \mu_i \frac{\partial^2 \mathcal{W}(x, c_i)}{\partial x_0^2}] \end{aligned} \right\}. \quad (52)$$

414 We may define $\eta_{max} = \max_{-d \leq x \leq d} |\eta(x)|$ as the maximum plate deflection and $\varepsilon_{max} = \max_{-d \leq x \leq d} \varepsilon(x)$ as

This is the author's peer reviewed, accepted manuscript. However, the online version of record will be different from this version once it has been copyedited and typeset.

PLEASE CITE THIS ARTICLE AS DOI: 10.1063/1.50198106

415 the maximum principal strain. η_{max}/A and $\varepsilon_{max}H/A$ versus the wave period τ are given in Fig. 4.
 416 In Fig. 4 (a), when $N_a = 0$, η_{max}/A initially increases with τ , and reaching a peak $\eta_{max}/A \approx$
 417 1.085 at $\tau \approx 18.4$. Subsequently, it gradually declines and approaches 1. By contrast, when an
 418 internal pin is added ($N_a = 1$), in addition to the region near the peaks of η_{max}/A , it can be found
 419 that η_{max}/A becomes much smaller in most range of τ . As N_a becomes larger, η_{max}/A further
 420 declines. When $N_a \geq 4$, η_{max}/A can even be close to zero. In Fig. 4(b), $\varepsilon_{max}H/A$ at $N_a = 1$ is
 421 normally greater than that at $N_a = 0$. However, when $N_a \geq 2$, the strain level becomes smaller than
 422 that without any pin. Besides, $\varepsilon_{max}H/A$ is further declined as N_a further increases.

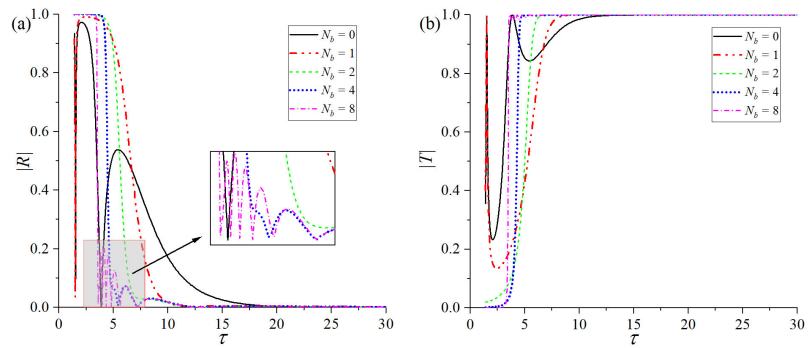
423

424 **2. All internal constraints are hinged supports**

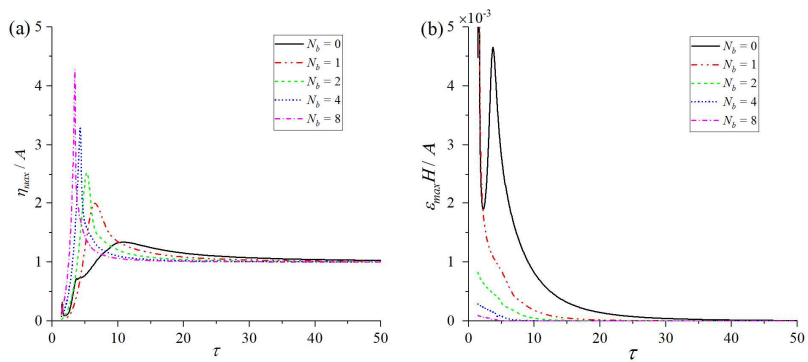
425 We may also consider the scenario floating elastic panels connected by internal hinges ($N_a = N_c =$
 426 0), where the positions b_i ($i = 1 \sim N_b$) of the internal hinges are assumed to present in the same
 427 distribution as the pins in Eq. (50), and two side edges at $x = \pm d$ are set to be free. The results of
 428 the reflection and transmission coefficients are given in Fig. 5. It can be observed that as N_b
 429 increases, the curves of $|R|$ and $|T|$ are significantly changed, which indicates that $|R|$ and $|T|$ are
 430 quite sensitive to N_b . Typically, at $N_b = 4$, a local oscillation of $|R|$ versus τ is observed, and such
 431 behaviour becomes much more evident at $N_b = 8$, as shown in the local enlargement in Fig. 5(a).
 432 The results of the maximum deflection and principal strain of the elastic plate are presented in Fig.
 433 6. In Fig. 6(a), η_{max}/A at each N_b generally shows a similar variation trend. In particular, η_{max}/A
 434 first increases with τ , and peaks at $\tau = 10.80, 6.50, 5.30, 4.26$ and 3.46 with $\eta_{max}/A = 1.34,$
 435 $1.99, 2.54, 3.28$ and 4.28 for $N_b = 0, 1, 2, 4, 8$ respectively. Subsequently, η_{max}/A gradually
 436 decreases and approaches 1 with the increase of τ . Notably, there is a positive correlation between
 437 the spike value and N_b . In Fig. 6(b), the introduction of additional hinged supports on the plate
 438 generally leads to a decrease in $\varepsilon_{max}H/A$. To clearly illustrate the behaviour of plate deflection at
 439 the spikes depicted in Fig. 6(a), the corresponding $|\eta(x)|$ versus x/d is plotted in Fig. 7. It can be
 440 observed that η_{max} in all the cases are occurred at $x = -d$. The profiles of $|\eta(x)|/A$ exhibit a
 441 degree of similarity across different values of N_b . In particular, $|\eta(x)|/A$ shows alternating
 442 variation with x/d with N_b troughs and $N_b + 2$ peaks. These peaks are located at the edges of each
 443 panel, and the corresponding peak values decrease as x/d . Moreover, at $N_b = 1$, obvious bending
 444 is observed in both 2 panels. However, as N_b increases, the bending in each plate is unobvious, and

This is the author's peer reviewed, accepted manuscript. However, the online version of record will be different from this version once it has been copyedited and typeset.
 PLEASE CITE THIS ARTICLE AS DOI: 10.1063/1.50198106

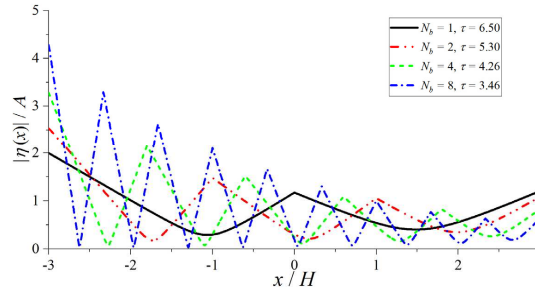
445 the entire structure performs like a series of rigid plates, which indicates that the elasticity of the
 446 structure becomes less important.



447
 448 Fig. 5. The reflection and transmission coefficients versus the wave period under different
 449 numbers of internal hinges: (a). reflection coefficients; (b). transmission coefficients. Here, two
 450 edges at $x = \pm d$ are free, $N_a = N_c = 0$.



451
 452 Fig. 6. The maximum deflection and principal strain in the elastic plates connected by one or
 453 multiple internal hinges: (a) maximum deflection; (b). maximum principal strain. Here, two edges
 454 at $x = \pm d$ are free, $N_a = N_c = 0$.



455

456

457

458

459

460

461

462

463

464

465

466

467

468

469

470

471

472

473

474

475

Fig. 7. Deflection of the elastic plate. Here, two edges at $x = \pm d$ are free, $N_a = N_c = 0$.

3. All internal constraints are free

Wave diffraction by multiple floating elastic panels without any connection is also considered ($N_a =$

$N_b = 0$). The reflection and transmission coefficients are presented in Fig. 8. Similar with the

phenomenon observed in Fig. 5, it can be found that $|R|$ and $|T|$ are also very sensitive to the

number of internal free edges N_c . As N_c increases, local oscillations on $|R|$ and $|T|$ versus τ are

also observed, such phenomenon is consistent with the results for an elastic plate of infinite extent

with multiple cracks³⁰. Compared with Fig. 5 for plates connected with hinges, the local oscillation

here is much stronger. In fact, such local oscillatory behaviour is due to the multiple reflections of

the traveling waves between two edges of the plate. With less restriction on the edge conditions, the

energy conversion between waves and plate motion is much more flexible, and may be sensitive to

the properties of ocean waves. Such conversion results in rapid variations of the energy in the

corresponding radiated and diffracted waves, thereby leading to more pronounced oscillation

phenomena. Consequently, in scenarios of free edges, more evident oscillatory behaviour in terms

of reflection and transmission coefficients is expected. In Fig. 9(a), obvious spikes can be observed

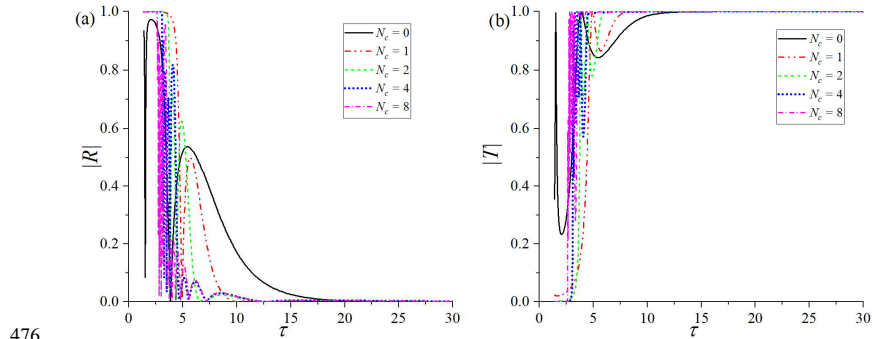
in the curves of η_{max}/A versus τ , and these peak values increase with N_c , which is similar with the

phenomenon in Fig. 6 (a). However, there is also a highly local oscillation near the peak, a feature

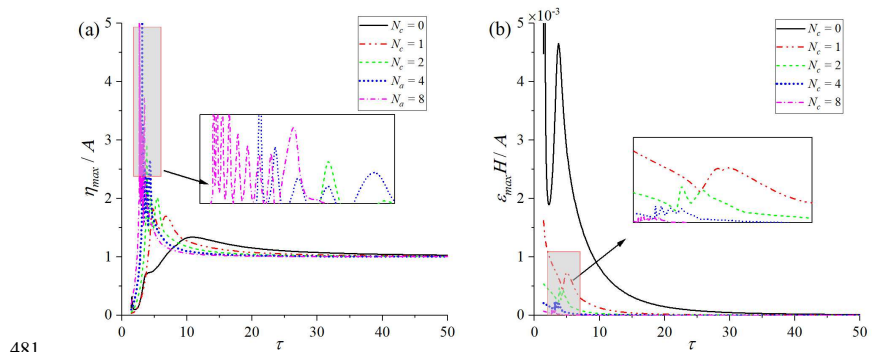
that markedly diverges from that in Fig. 6(a). $\varepsilon_{max}H/A$ in Fig. 9(b) generally decreases with N_c at

a fixed τ . Besides, a weak local oscillation is also observed in $\varepsilon_{max}H/A$ versus τ as N_c increases.

This is the author's peer reviewed, accepted manuscript. However, the online version of record will be different from this version once it has been copyedited and typeset.
 PLEASE CITE THIS ARTICLE AS DOI: 10.1063/5.0198106



476
 477 Fig. 8. The reflection and transmission coefficients versus the wave period under different
 478 numbers of internal free edges: (a). reflection coefficients; (b). transmission coefficients. Here,
 479 two edges at $x = \pm d$ are free, $N_a = N_b = 0$.
 480



481
 482 Fig. 9. The maximum deflection and principal strain in the elastic plates with free edge conditions:
 483 (a). maximum deflection; (b). maximum principal strain. Here, two edges at $x = \pm d$ are free,
 484 $N_a = N_b = 0$.
 485

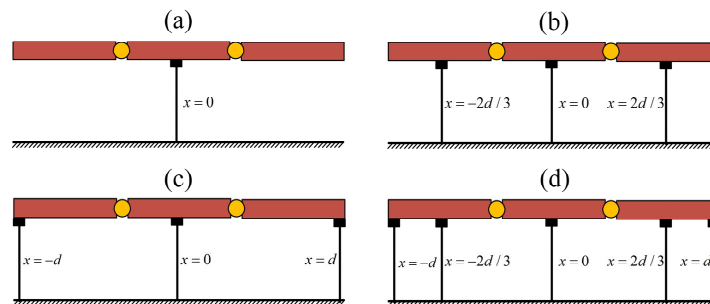
486 **C. Wave interaction with floating elastic plates with different type of internal constraints**

487 In actual engineering structures, each of the panel components can be designed to be connected by
 488 certain edge conditions, and mooring lines are usually used to improve the stability of the entire
 489 structure. Hence, considering the combined effects of various types of physical constraints on the
 490 hydrodynamic properties of the structure is quite necessary. Here, we may consider a scenario that
 491 three identical elastic plates are connected by two hinges ($b_1 = -d/3, b_2 = d/3$), and we try to

This is the author's peer reviewed, accepted manuscript. However, the online version of record will be different from this version once it has been copyedited and typeset.

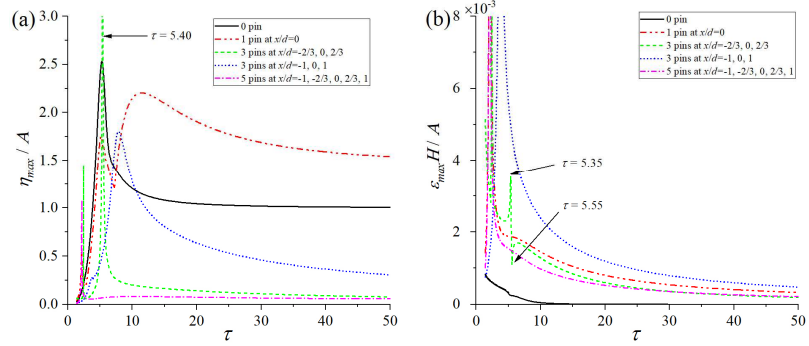
PLEASE CITE THIS ARTICLE AS DOI: 10.1063/1.50198106

492 arrange pinned supports on these plates to reduce the maximum deflection and principal strain in
 493 the structure, which can be regarded as a theoretical study to optimize the mooring positions for a
 494 series of hinged floating elastic plates. Here, four different configurations are considered, as shown
 495 in Fig. 10. The corresponding results are given in Fig. 11. In Fig. 11(a), if only one pinned support
 496 is imposed at $x = 0$ (Fig. 10 (a)), compared with the case without any pin, η_{max}/A becomes even
 497 much larger over a wide range of τ , which is different from the result for a single plate in Fig. 4 (a).
 498 By contrast, Fig. 11 (a) also indicated that the other three configurations in Fig. 10 can effectively
 499 mitigate the magnitude of η_{max}/A . In particular, apart from some narrow peaks in η_{max}/A when τ
 500 is small, the configuration in Fig. 10 (d) emerges as the most effective, followed by the configuration
 501 in Fig. 10 (b), and subsequently Fig. 10 (c). For the maximum principal strain on the plate given in
 502 Fig. 11 (b), it is observed that every configuration in Fig. 10 results in an increase of $\epsilon_{max}H/A$,
 503 across a wide range of τ , compared to the scenario without any pinned support. However, the
 504 increase is relatively less under the configurations presented in Figs. 10(b) and (d). Furthermore,
 505 Fig. 11(b) reveals a marked and rapid variation in $\epsilon_{max}H/A$ within the range of $5.35 \leq \tau \leq 5.55$
 506 under the configuration in Fig. 10 (b), and it is associated with the spike on η_{max}/A in Fig. 11(a).
 507 Correspondingly, this phenomenon is also reflected in the deflection and principal strain
 508 distributions in the plate, as illustrated in Fig. 12. Besides, we also observe that η_{max}/A is maximum
 509 at $x = \pm d$ and $x = \pm d/2$ with a close value, and $\epsilon_{max}H/A$ is maximum at the pinned positions at
 510 $x = \pm 2d/3$.

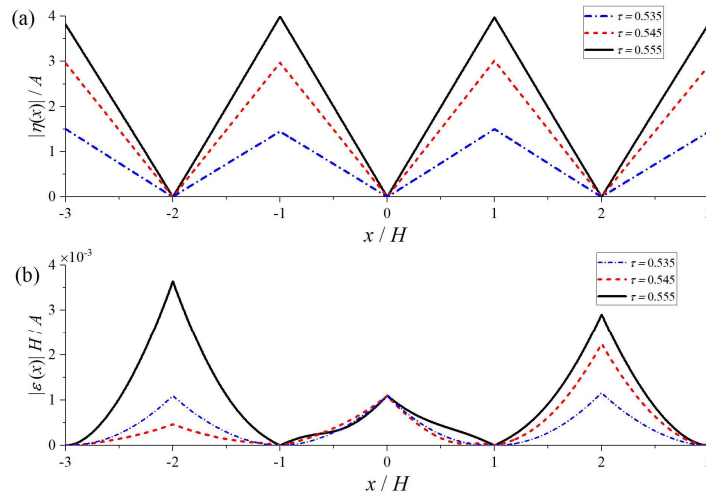


511
 512 Fig. 10. Four different schemes to arrange pinned supports. (a) $a_1 = 0$; (b) $a_1 = -\frac{2d}{3}$, $a_2 = 0$,
 513 $a_3 = \frac{2d}{3}$; (c) $a_1 = -d$, $a_2 = 0$, $a_3 = d$; (d) $a_1 = -d$, $a_2 = -\frac{2d}{3}$, $a_3 = 0$, $a_4 = \frac{2d}{3}$, $a_5 = d$.

This is the author's peer reviewed, accepted manuscript. However, the online version of record will be different from this version once it has been copyedited and typeset.
 PLEASE CITE THIS ARTICLE AS DOI: 10.1063/5.0198106



514
 515 Fig. 11. The maximum deflection (a) and principal strain (b) in the elastic plates corresponding to
 516 the configurations in Fig. 10.



517
 518 Fig. 12. Deflection (a) and distribution of the principal strain (b) of the elastic plate. Two edges at
 519 $x = \pm d$ are free, $N_a = 3$ with $a_1 = -\frac{2d}{3}$, $a_2 = 0$, $a_3 = \frac{2d}{3}$, $N_b = 2$ with $b_1 = -\frac{d}{3}$, $b_2 = \frac{d}{3}$, $N_c =$
 520 0.

522 **V. CONCLUSION**

523 The problem of wave interaction with multiple adjacent floating solar panels with three different
 524 types of constraints is considered, namely pinned, hinged and free. The solution procedure is based
 525 on a domain decomposition methodology, where the velocity potential of the fluid beneath the solar

This is the author's peer reviewed, accepted manuscript. However, the online version of record will be different from this version once it has been copyedited and typeset.

PLEASE CITE THIS ARTICLE AS DOI: 10.1063/1.50198106

526 panels is constructed through the boundary integral equation by invoking the Green function for
 527 fluid fully covered by an elastic plate. The velocity potential in the free surface domain is expanded
 528 as a conventional infinite series by using vertical mode expansion. Such an approach makes the
 529 computation much more effective, since the unknown coefficients only need to be distributed on
 530 two interfaces, as well as the jumps of physical parameters of the plates.

531

532 Based on the developed scheme, the effects of three constraints on the elastic plates are extensively
 533 investigated. It is found that pinned supports can increase (decrease) the reflection coefficient $|R|$
 534 (transmission coefficient $|T|$) for long waves. With the number of pinned supports increases, the
 535 magnitude of maximum deflection η_{max} and principal strain ε_{max} in the plates can be reduced. For
 536 multiple adjacent floating elastic panels connected by hinges or free to each other, it is observed that
 537 $|R|$ and $|T|$ are quite sensitive to the number of edges. Besides, a local oscillation will be apparent
 538 in the curves of $|R|$ and $|T|$ versus wave period τ , and such a phenomenon is much more evident in
 539 the case of free edges. This local oscillation can be attributed to the lesser restriction at the free
 540 edges of the plates, resulting in a stronger energy conversion between transmitted and radiated
 541 waves. Furthermore, with the increase of the number of edges, spikes in the curve of η_{max} versus τ
 542 become more pronounced, as well as ε_{max} is generally decreased.

543

544 The combined influence of hinged and pinned supports on the hydrodynamic response of multiple
 545 floating elastic plates is also evaluated. A case study is conducted for three identical elastic plates
 546 connected by hinged plates. Four distinct configurations with varying pinned points are considered.
 547 The analysis revealed that the placement of pinned supports has a considerable impact on both η_{max}
 548 and ε_{max} . In some instances, additional pinned supports even result in an increase in η_{max} . The
 549 present investigation provides a theoretical attempt to the optimization of mooring positions on
 550 floating solar panels.

551

552 Although only three typical edge conditions are considered in the present study, the solution
 553 procedure can be easily extended to other types of constraints by changing the jump terms in the
 554 boundary integral equation.

555

This is the author's peer reviewed, accepted manuscript. However, the online version of record will be different from this version once it has been copyedited and typeset.

PLEASE CITE THIS ARTICLE AS DOI: 10.1063/5.0198106

556 **ACKNOWLEDGMENTS**

557 This work is supported by the National Natural Science Foundation of China (Grant No. 52271276).
 558 KR acknowledges funding support from the Royal Society (IEC\NSFC\223358), and from the
 559 Lloyds Register Foundation (N21\100005). LFH acknowledges grants from Innovate UK (No.
 560 10048187, 10079774, 10081314) and the Royal Society (IEC\ NSFC\ 223253, RG\R2\232462).

561

562 **DATA AVAILABILITY STATEMENT**

563 The data that supports the findings of this study is available within the article.

564

565 **REFERENCES**

- 566 ¹IRENA, How falling costs make renewables a cost-effective investment Document No. Number, 2020.
 567 ²R. M. Almeida, R. Schmitt, S. M. Grodsky, A. S. Flecker, C. P. Gomes, L. Zhao, H. Liu, N. Barros, R.
 568 Kelman, and P. B. McIntyre, "Floating solar power could help fight climate change—let's get it right,"
 569 *Nature* **606**, 246 (2022).
 570 ³T. Hooper, A. Armstrong, and B. Vlaswinkel, "Environmental impacts and benefits of marine floating
 571 solar," *Solar Energy* **219**, 11 (2021).
 572 ⁴C. Fox, and V. A. Squire, "Reflection and transmission characteristics at the edge of shore fast sea ice,"
 573 *Journal of Geophysical Research: Oceans* **95**, 11629 (1990).
 574 ⁵N. J. Balmforth, and R. V. Craster, "Ocean waves and ice sheets," *J. Fluid Mech.* **395**, 89 (1999).
 575 ⁶M. H. Meylan, and V. A. Squire, "The response of ice floes to ocean waves," *Journal of Geophysical*
 576 *Research: Oceans* **99**, 891 (1994).
 577 ⁷C. Wu, E. Watanabe, and T. Utsunomiya, "An eigenfunction expansion-matching method for analyzing
 578 the wave-induced responses of an elastic floating plate," *Applied Ocean Research* **17**, 301 (1995).
 579 ⁸I. V. Sturova, "Diffraction of surface waves on an inhomogeneous elastic plate," *Journal of Applied*
 580 *Mechanics and Technical Physics* **41**, 612 (2000).
 581 ⁹D. V. Evans, and R. Porter, "Wave scattering by narrow cracks in ice sheets floating on water of finite
 582 depth," *J. Fluid Mech.* **484**, 143 (2003).
 583 ¹⁰T. D. Williams, and V. A. Squire, "Scattering of flexural-gravity waves at the boundaries between three
 584 floating sheets with applications," *J. Fluid Mech.* **569**, 113 (2006).
 585 ¹¹H. Chung, and C. Fox, "Calculation of wave-ice interaction using the Wiener-Hopf technique," *New*
 586 *Zealand J. Math* **31**, 1 (2002).
 587 ¹²Y. Shi, Z. F. Li, and G. X. Wu, "Interaction of wave with multiple wide polynyas," *Phys. Fluids* **31**,
 588 067111 (2019).
 589 ¹³K. Ren, G. X. Wu, and G. A. Thomas, "Wave excited motion of a body floating on water confined
 590 between two semi-infinite ice sheets," *Phys. Fluids* **28**, 127101 (2016).
 591 ¹⁴D. Karmakar, and C. G. Soares, "Scattering of gravity waves by a moored finite floating elastic plate,"
 592 *Applied Ocean Research* **34**, 135 (2012).
 593 ¹⁵S. C. Mohapatra, R. Ghoshal, and T. Sahoo, "Effect of compression on wave diffraction by a floating
 594 elastic plate," *Journal of Fluids and Structures* **36**, 124 (2013).

This is the author's peer reviewed, accepted manuscript. However, the online version of record will be different from this version once it has been copyedited and typeset.

PLEASE CITE THIS ARTICLE AS DOI: 10.1063/5.0198106

- 595 ¹⁶D. Karmakar, J. Bhattacharjee, and T. Sahoo, "Wave interaction with multiple articulated floating
596 elastic plates," *Journal of Fluids and Structures* **25**, 1065 (2009).
- 597 ¹⁷K. M. Praveen, D. Karmakar, and C. Guedes Soares, "Hydroelastic analysis of periodic arrays of
598 multiple articulated floating elastic plate," *Ships and Offshore Structures* **15**, 280 (2020).
- 599 ¹⁸C. W. Zhang, P. F. Wang, L. F. Huang, M. K. Zhang, H. T. Wu, and D. Z. Ning, "Resonance mechanism
600 of hydroelastic response of multi-patch floating photovoltaic structure in water waves over stepped
601 seabed," *Phys. Fluids* **35**, (2023).
- 602 ¹⁹V. A. Squire, "Of ocean waves and sea-ice revisited," *Cold Regions Science and Technology* **49**, 110
603 (2007).
- 604 ²⁰V. A. Squire, "Synergies between VLFS hydroelasticity and sea ice research," *International Journal of*
605 *Offshore and Polar Engineering* **18**, (2008).
- 606 ²¹Y. F. Yang, G. X. Wu, and K. Ren, "Three-dimensional interaction between uniform current and a
607 submerged horizontal cylinder in an ice-covered channel," *J. Fluid Mech.* **928**, A4 (2021).
- 608 ²²K. Ren, G. X. Wu, and Y. F. Yang, "Surface wave interaction with floating elastic plates in channels,"
609 *Phys. Fluids* **36**, (2024).
- 610 ²³R. Eatock Taylor, "Hydroelastic analysis of plates and some approximations," *Journal of engineering*
611 *mathematics* **58**, 267 (2007).
- 612 ²⁴Z. F. Li, G. X. Wu, and C. Y. Ji, "Wave radiation and diffraction by a circular cylinder submerged below
613 an ice sheet with a crack," *J. Fluid Mech.* **845**, 682 (2018).
- 614 ²⁵T. Sahoo, T. L. Yip, and A. T. Chwang, "Scattering of surface waves by a semi-infinite floating elastic
615 plate," *Phys. Fluids* **13**, 3215 (2001).
- 616 ²⁶Y. F. Yang, G. X. Wu, and K. Ren, "Hydroelastic wave diffraction by a vertical circular cylinder
617 standing in a channel with an ice cover," *J. Fluid Mech.* **941**, A13 (2022).
- 618 ²⁷D. W. Xia, J. W. Kim, and R. C. Ertekin, "On the hydroelastic behavior of two-dimensional articulated
619 plates," *Marine structures* **13**, 261 (2000).
- 620 ²⁸B. Noble, and G. Weiss, "Methods based on the Wiener-Hopf technique for the solution of partial
621 differential equations," *Phys. Today* **12**, 50 (1959).
- 622 ²⁹S. P. Timoshenko, and S. Woinowsky-Krieger, *Theory of plates and shells* (McGraw-hill, 1959).
- 623 ³⁰R. Porter, and D. V. Evans, "Scattering of flexural waves by multiple narrow cracks in ice sheets floating
624 on water," *Wave Motion* **43**, 425 (2006).
- 625